Vol. 93 (1997) ACTA PHYSICA POLONICA A No. 2

Proceedings of the 1st International Symposium on Scanning Probe Spectroscopy and Related Methods, Poznań 1997

ELECTRONIC PHASE TRANSITION IN LAYERED MATERIALS $1T$-TaS_xSe_{2-x} PROBED BY CRYOGENIC STM/STS

T. HASEGAWA

Materials and Structures Laboratory, Tokyo Institute of Technology
Nagatsutacho 4259, Midori-ku, Yokohama 226, Japan

O. SHIINO, W. YAMAGUCHI, T. ENDO, H. SUGAWARA AND K. KITAZAWA

Department of Applied Chemistry, University of Tokyo
Japan Science and Technology Corporation
Hongo 7-3-1, Bunkyo-ku, Tokyo 113, Japan

A metal–insulator transition, Mott transition, in layered materials $1T$-TaS_xSe_{2-x} was investigated by cryogenic scanning tunneling microscopy/spectroscopy. At 77 K, tunneling spectra in the insulating phase showed a conduction band with almost half filling, which becomes narrower as x decreases. Around the transition point $x \approx 1.4$ at 77 K, we observed a sign of gap opening without an overshooting peak at zero bias, supporting the Mott localization picture in which a carrier number vanishes at the transition point. From the site-specified scanning tunneling spectroscopy measurements, furthermore, electrons were found to localize at the charge density wave crest positions. In $1T$-TaS_2, we have also found that both metallic and insulating phases coexist in a nanometer scale just above the transition temperature, 180 K. From the minimum size of the insulating region, the coherence length of Mott insulating state was evaluated to be ≈ 5 nm.

PACS numbers: 71.30.+h, 71.20.–b

1. Introduction

Motivated by the establishment that high temperature superconductivity appears by doping carriers into Mott insulating compounds, electronic states in the neighborhood of metal–Mott insulator phase boundary have been extensively studied so far. The transitional Mott transition theory based on the Hubbard model starts from a half-filled band. That is, each atomic lattice site emits one conducting electron. As the on-site Coulomb interaction U becomes larger or the transfer t becomes smaller, electron effective mass, m^*, increases and diverges to infinity, and the system is transformed to an insulating state [1]. As approaching

the Mott transition point from the metallic side, one observes a sharp peak at the Fermi energy E_F in the density of states (DOS) vs. energy profile. In the insulating phase, the original single band splits into upper and lower Hubbard bands separated with a finite energy gap.

Recently, however, Imada [2] pointed out that there is another possibility in Mott transition that a carrier number, n, goes to zero near the transition point, since electrical conductivity σ is proportional to n/m^*. According to this mechanism, the density of states at E_F, $N(0)$, rapidly diminishes without indicating a narrow peak at E_F.

Scanning tunneling microscopy/spectroscopy (STM/STS) is a powerful technique to investigate changes in low energy excitation spectra associated with phase transition, because of its superior energy resolution, which is actually limited by the thermal smearing effect, k_BT, and has been applied to various electronic phase transition phenomena, such as superconductivity [3], charge density wave (CDW) formation [4–7], and Mott transition [8–10]. Kim et al. [8] reported site-specified STS measurements on $1T$-TaS_2 in the Mott insulator phase, at 77 K, and concluded that the local density of states was transferred from the CDW trough sites to crest site, giving a clear evidence that the Mott localization occurs in $1T$-TaS_2.

Here, we performed variable temperature STM/STS measurements on the solid solution system $1T$-TaS_xSe_{2-x}, focusing on the compositional dependence at 77 K and the temperature dependence for $1T$-TaS_2. From the site-specified tunneling spectra, the parameters which govern the transition will be discussed on the basis of Mott–Hubbard model.

2. Experimental

A series of single crystal specimens $1T$-TaS_xSe_{2-x} was grown by the conventional vapor transport method using iodine as an agent. Resistivity vs. temperature curves recorded for the synthesized crystals are summarized in Fig. 1 [11]. At 77 K, resistivity abruptly jumps at the composition $x \approx 1.4$, corresponding to the Mott

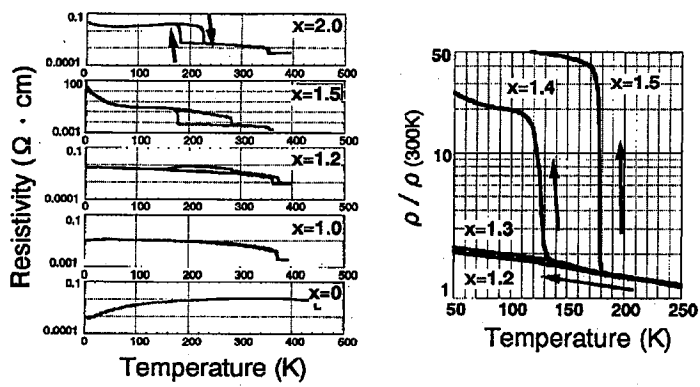

Fig. 1. Resistivity vs. temperature curves for $1T$-TaS_xSe_{2-x}.

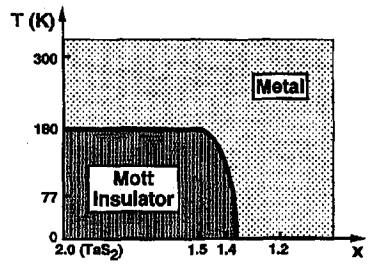

Fig. 2. Electronic phase diagram for $1T$-TaS_xSe_{2-x}.

transition. In $1T$-TaS_2, a metal–insulator transition takes place at 180 K in the cooling process. The electronic phase diagram deduced from the resistivity data is illustrated in Fig. 2.

In the present study, a home-made variable temperature UHV-STM instrument was utilized. Just prior to the STM/STS observations, the single crystal specimens were cleaved in UHV. All STM measurements were performed with the constant current mode.

3. Results and discussion

3.1. Compositional dependence of tunneling spectrum at 77 K

Figure 3a shows a STM image of $1T$-$TaSe_2$ obtained at 77 K, where the black spots represent the locations at which tunneling spectroscopic measurements were performed simultaneously with STM scanning [9]. Figures 3b and c plot site-specified tunneling spectra taken at the CDW crest and trough positions, respectively. As can be seen, there are three bands separated by small gaps at $V = -600$ mV and $+400$ mV. Furthermore, it is notable that the central band lying on E_F is almost half-filled.

In $1T$-TaS_xSe_{2-x} without CDW modulation, a Ta $5d$ band possesses one electron per one Ta atom. The CDW modulation forms so-called star of David structures, consisting of 13 Ta atoms, and thus, the original $5d$ band splits into 13 subbands. Since odd numbers of Ta atoms are included in a $\sqrt{13} \times \sqrt{13}$ unit cell, the reconstructed conduction band is hall-filled [12]. That is, $1T$-TaS_xSe_{2-x} with CDW modulation should be metallic, as well. According to the band calculation in which sinusoidal CDW modulation is taken into account, the subbands composes three manifolds, spaced with CDW gaps [13].

Therefore, the tunneling conductance data of $1T$-$TaSe_2$ in Fig. 3 is quantitatively consistent with the band picture, described above. Namely, a narrow conduction band, apart from higher and lower energy bands, is nearly half-filled, although the location of the conduction band is shifted toward a lower energy side in comparison with the band prediction.

Figures 4a and b show STM images taken for $1T$-$TaS_{1.4}Se_{0.6}$ at room temperature and 77 K, respectively. At room temperature, the CDW superstructure is well arranged, and the background level is rather flat, indicating that the surface electronic states is relatively homogeneous. At 77 K, in contrast, we frequently

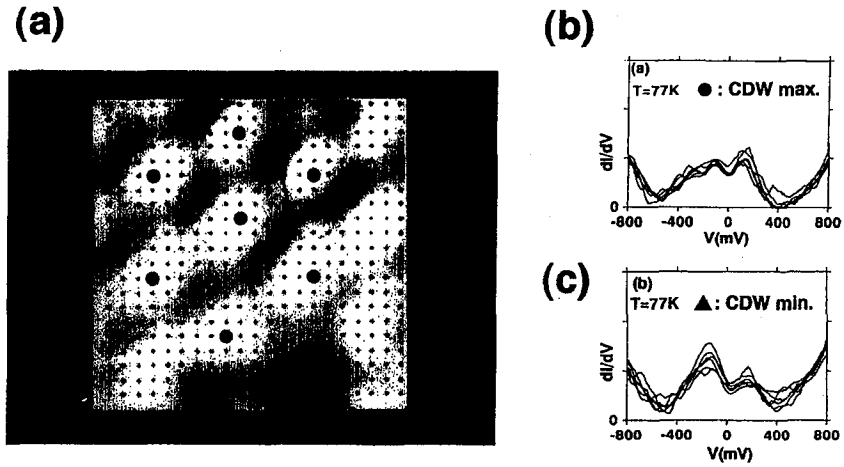

Fig. 3. STS results for $1T$-$TaSe_2$ at 77 K. (a) STM image taken with the STS mode, where black dots represent the spectroscopic measurement locations, (b) tunneling spectra observed at the CDW crest positions, (c) tunneling spectra observed at the CDW trough positions.

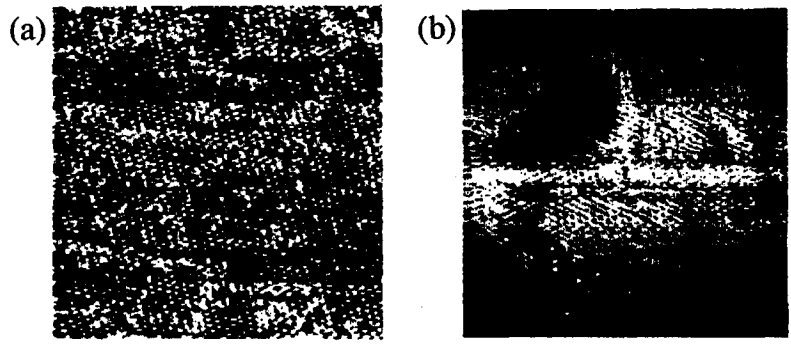

Fig. 4. STM image of $1T$-$TaS_{1.4}Se_{0.6}$ at (a) room temperature and (b) 77 K. Bias voltages and set-point currents are 50 mV and 0.25 nA, respectively.

encountered less conducting regions, around which the CDW modulation is disturbed, suggesting occurrence of electronic phase separation at low temperatures. Corresponding to the inhomogeneous electronic nature at 77 K, the observed tunneling spectra showed a wide variety, particularly in the shape of conduction band, as exhibited in Fig. 5. From the figure, one can clearly see signs of band splitting and gap opening.

The band width B, which is proportional to the transfer integral t, and the U parameter in the Hubbard model, estimated as the peak to peak separation energy [1], are plotted as functions of x in Fig. 6a. The B value for $x \approx 1.4$ is fairly smaller than that for $x = 0$, suggesting that t decreases with increasing x. For $x < 1.4$, moreover, U is rapidly enhanced with respect to x, although for $x > 1.4$

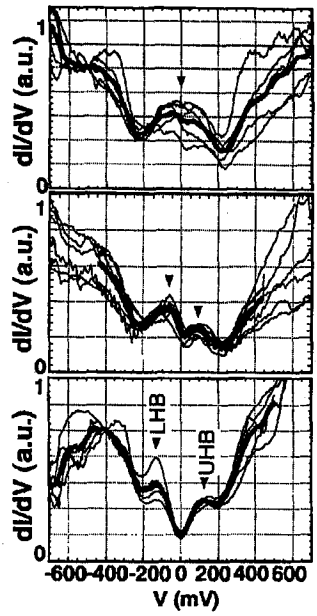

Fig. 5. Typical examples of tunneling spectra for $1T$-$TaS_{1.4}Se_{0.6}$ at 77 K.

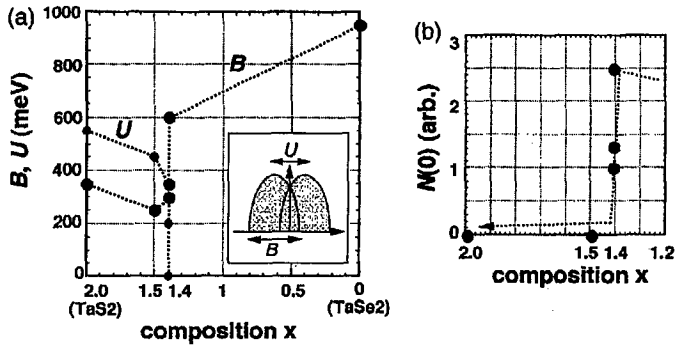

Fig. 6. B, U and $N(0)$ parameters as functions of x.

it cannot be evaluated from the tunneling spectra. In conclusion, the S substitution for Se increases, in a phenomenological sense, the parameter U/t, which drives the Mott transition.

As pointed out by Imada [2], there are two types of Mott transition; i.e., (1) electron effective mass, m^*, diverges to infinity, (2) carrier number, n, goes to zero. In the first case, corresponding to the original definition of Mott transition, a narrow peak is expected to emerge at E_F in the density of states profile [14–16]. In the second case, a half-filled band simply splits into two subbands without a mass enhancement peak, and the density of states at E_F, $N(0)$, is monotonously

lowered. The tunneling spectra for $x \approx 1.4$ do not show a zero bias conductance peak at all, supporting the second mechanism ($n \rightarrow 0$) for the Mott transition in the present system.

When measuring the tunneling spectra, the feedback loop was turned off and the high voltage applied to the z-axis piezo was hold. The obtained $I-V$ characteristics are automatically normalized at the bias voltage and set-point current so that in general the absolute DOS values cannot be compared between different spectra. In the present study, however, we estimated the $N(0)$ values relatively as a function of x, in the following way. The conduction band is well resolved from higher and lower bands, so that one can easily estimate the area of conduction band, S, in $\mathrm{d}I/\mathrm{d}V-V$ curves. According to Luttinger's theorem, S is conserved even if electron correlation is incorporated. By normalizing the tunneling spectra by S, the relative variation of $N(0)$ with x can be deduced. The resulting $N(0)$ vs. x plot, in Fig. 6b, evidently reveals that $N(0)$ is abruptly decreased around the transition point.

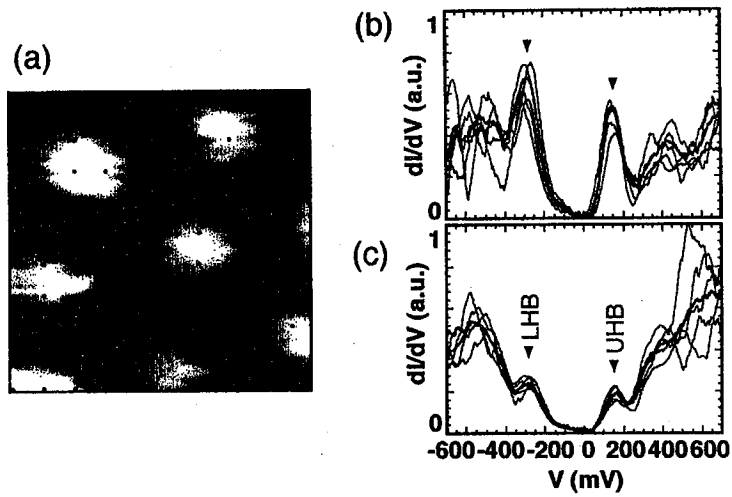

Fig. 7. STS results for $1T$-$TaS_{1.5}Se_{0.5}$ at 77 K. (a) STM image taken with the STS mode, (b) tunneling spectra observed at the CDW crest positions, (c) tunneling spectra observed at the CDW trough positions.

Figure 7 shows an STM image and site-specified tunneling spectra for the specimen $x = 1.5$ [10]. As can be seen, the tunneling spectra indicate a finite gap of ≈ 200 meV at E_F, implying that the Mott transition is completed. Moreover, the overshooting peaks at $V = -300$ mV and $+200$ mV, corresponding to lower and upper Hubbard bands, respectively, are synchronously enhanced at the locations of CDW crest. By comparing the areas of Hubbard bands, it is estimated that about 40% of local DOS (LDOS) is transferred from the CDW trough sites to crest sites in real space. In band insulators, in general, LDOS near the top of valence band is maximized at ionic lattice sites, while that near the bottom of conduction band is

minimized there. Therefore, the site-specified tunneling data in Fig. 7 give a direct evidence that Mott localization actually occurs in $1T$-$TaS_{1.5}Se_{0.5}$ [8].

3.2. Tunneling spectrum for $1T$-TaS_2 near the Mott transition temperature

Figure 8a is an STM image of $1T$-TaS_2 taken at 193 K, just above the Mott transition temperature. The figure exhibits two different regions with brighter and darker contrast. Figures 8b and c compare the tunneling spectra averaged over bright and dark regions in Fig. 8a. The bright region shows a metallic tunneling behavior with a finite $N(0)$ value, while in the dark region a Mott–Hubbard gap-like feature can be clearly seen, although the upper and lower Hubbard bands are substantially broadened, possibly due to the thermal smearing effect. This means that the metallic and Mott insulating phases could coexist in a nanometer scale near the transition point. In Fig. 8c, no zero bias conductance is detected, suggesting that the Mott transition in the present solid solution system is generally characterized by the feature $n \rightarrow 0$.

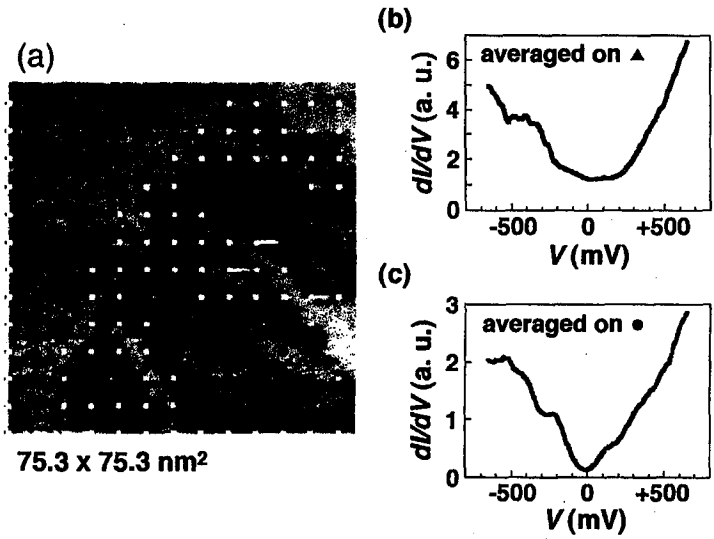

Fig. 8. STS results for $1T$-TaS_2 at 193 K. (a) STM image taken with the STS mode, (b) tunneling spectra observed on the bright region, (c) tunneling spectra observed on the dark regions.

Figure 9 shows an STM image including an isolated dark region with the minimum size of $\approx$ 5 nm. This value is considered to be equivalent to the coherence length of Mott localized state in $1T$-TaS_2, defined as the minimum spatial length required to destroy the Mott localization. To our knowledge, Fig. 9 is the first experimental observation directly indicating coherence length in a Mott localized state.

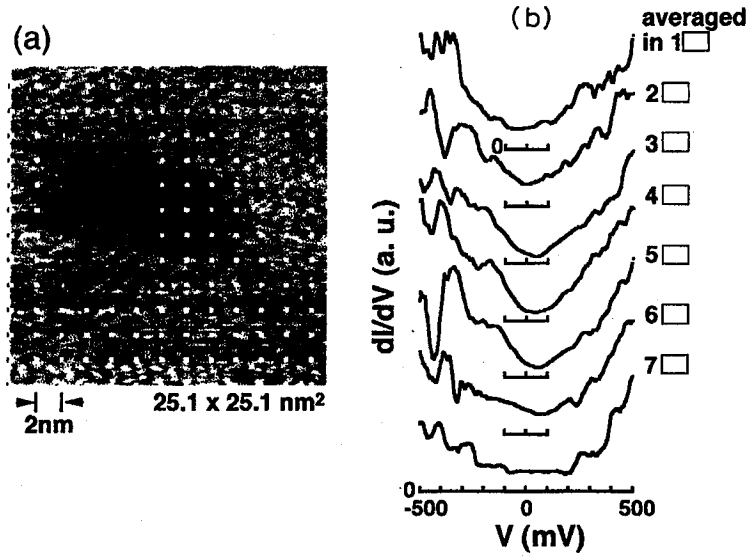

Fig. 9. STM results for $1T$-TaS_2 at 193 K. (a) STM image taken with the STS mode, (b) tunneling spectra observed at the locations marked as squares in the STM image.

4. Summary

In summary, we have performed STM/STS observations on a solid solution system $1T$-TaS_xSe_{2-x} near the Mott transition points. The electronic picture of metallic phase was qualitatively consistent with the band calculation, predicting that a narrow conduction band reconstructed by CDW formation is half-filled. From the compositional dependence of tunneling spectrum at 77 K, the S substitution for Se was found to cause an increase in U/t phenomenologically. Near $x = 1.4$, the electronic structure was rather inhomogeneous, and indicated a sign of band splitting without-a mass enhancement peak. This leads to the conclusion that a carrier number n is rapidly reduced near the transition. From the site-specified spectroscopic measurements, it was confirmed that approximately 40% of LDOS was transferred from the CDW trough sites to crest sites.

In $1T$-TaS_2, both metallic and Mott insulating phases could coexist just above the transition temperature. From the minimum size of insulating region, the coherence length of Mott localized states can be estimated to be ≈ 5 nm.

References

[1] N.F. Mott, *Metal–Insulator Transitions*, Taylor and Francis, London 1974.

[2] M. Imada, *J. Phys. Soc. Jpn.* **62**, 1105 (1993).

[3] T. Hasegawa, H. Ikuta, K. Kitazawa, in: *Physical Properties of High Temperature Superconductors III*, Ed. D.M. Ginsberg, World Scientific, Singapore 1992, p. 525.

[4] J.A. Wilson, F.J. DiSalvo, S. Mahasan, *Adv. Phys.* **24**, 117 (1975).

[5] R.V. Coleman, B. Drake, P.K. Hansma, C.G. Slough, *Phys. Rev. Lett.* **55**, 394 (1985).

[6] R.V. Coleman, B. Drake, P.K. Hansma, A. Johnson, W.W. McNairy, C.G. Slough, *Adv. Phys.* **37,** 559 (1988).

[7] W. Wang, B. Giambattista, C.G. Slough, R.V. Coleman, M.A. Subramaniam, *Phys. Rev. B* **42,** 8890 (1990).

[8] J.-J. Kim, W. Yamaguchi, T. Hasegawa, K. Kitazawa, *Phys. Rev. Lett.* **73,** 2103 (1994).

[9] J.-J. Kim, W. Yamaguchi, T. Hasegawa, K. Kitazawa, *Phys. Rev. B* **50,** 4958 (1994).

[10] O. Shiino, T. Endo, W. Yamaguchi, H. Sugawara, T. Hasegawa, K. Kitazawa, *Czech. J. Phys.* **46,** 2621 (1996).

[11] F.J. DiSalvo, J.A. Wilson, B.G. Bagley, J.V. Waszczak, *Phys. Rev. B* **12,** 2220 (1975).

[12] P. Fazekas, E. Tosatti, *Physica B* **99,** 183 (1980).

[13] N.V. Smith, S.D. Kevan, F.J. DiSalvo, *J. Phys. C* **18,** 3173 (1985).

[14] A. Georges, W. Krauth, *Phys. Rev. B* **48,** 7167 (1993).

[15] Y. Tokura, Y. Taguchi, Y. Okada, Y. Fujishima, T. Arima, K. Kumagai, Y. Iye, *Phys. Rev. Lett.* **70,** 2126 (1993).

[16] M.J. Rozenberg, I.H. Inoue, H. Makino, F. Iga, Y. Nishihara, *Phys. Rev. Lett.* **76,** 4781 (1996).